






Nonlocal quantum heat engines made of hybrid superconducting devices

S. Mojtaba Tabatabaei ¹, David Sánchez ², Alfredo Levy Yeyati ³, and Rafael Sánchez ³

¹*Department of Physics, Kharazmi University, 15719-14911 Tehran, Iran*

²*Institute for Cross-Disciplinary Physics and Complex Systems IFISC (UIB-CSIC), E-07122 Palma de Mallorca, Spain*

³*Departamento de Física Teórica de la Materia Condensada, Condensed Matter Physics Center (IFIMAC), and Instituto Nicolás Cabrera, Universidad Autónoma de Madrid, 28049 Madrid, Spain*

 (Received 18 July 2022; revised 30 August 2022; accepted 31 August 2022; published 15 September 2022)

We discuss a quantum thermal machine that generates power from a thermally driven double quantum dot coupled to normal and superconducting reservoirs. Energy exchange between the dots is mediated by electron-electron interactions. We can distinguish three main mechanisms within the device operation modes. In the Andreev tunneling regime, energy flows in the presence of coherent superposition of zero- and two-particle states. Despite the intrinsic electron-hole symmetry of Andreev processes, we find that the heat engine efficiency increases with increasing coupling to the superconducting reservoir. The second mechanism occurs in the regime of quasiparticle transport. Here we obtain large efficiencies due to the presence of the superconducting gap and the strong energy dependence of the electronic density of states around the gap edges. Finally, in the third regime there exists a competition between Andreev processes and quasiparticle tunneling. Altogether, our results emphasize the importance of both pair tunneling and structured band spectrum for an accurate characterization of the heat engine properties in normal-superconducting coupled dot systems.

DOI: [10.1103/PhysRevB.106.115419](https://doi.org/10.1103/PhysRevB.106.115419)

I. INTRODUCTION

Thermoelectric effects in solid state devices allow us to convert heat exchanged with the environment into an electric current. Nanoscale conductors can this way work as on-chip converters of waste heat into power at low temperatures [1]. To this end, a mechanism that breaks particle-hole symmetry is needed. Among the desired properties of a good thermoelectric engine, the conductor should be electrically isolated from the thermal source, such that the absorbed heat and the generated charge currents are well separated as is the case, e.g., in a thermocouple. Despite the fact that superconductors are good thermal insulators and (obviously) good electrical conductors [2], they are rarely considered as components of thermoelectric generators due to their intrinsic electron-hole symmetry [3].

Recent approaches to this problem exploit tunnel junctions between unequal superconducting electrodes using nonlinearities [4–6] or single-electron transistors [7–9], hybrid normal-superconductor junctions including quantum dot energy filters [10–15], spin-dependent scattering [16–26], photon-assisted tunneling [27], or interference phenomena [28,29]. The gapped density of states has also been successfully used for cooling [30,31] and for power sources [32,33].

Mesoscopic versions of the thermocouple geometry are based on three terminal configurations, where one terminal acts as the thermal reservoir and the other two support the charge current. The coupling to the heat source must be such that no particle currents are injected in the conductor, at least on average. Different mechanisms have been proposed depending on the way carriers couple to the heat source. This coupling can be mediated by microscopic interactions, e.g.,

charge correlations [34–39] and electron-boson interactions [40–52], or due to electronic relaxation in hot probes [53–57], to mention a few quantum dot systems. Of particular interest are heat engines based on capacitively coupled dots [58–61], where the separation of charge and heat currents is explicit: current flows in one conductor, that we call passive, with the other one being connected to the heat source via charge fluctuations [34–38,62–67]. Reversely the charge current (in response to a voltage bias or to temperature differences) can be used to operate the system as a refrigerator [68–73].

Similar coupling schemes are relevant for mesoscopic Coulomb drag configurations [74–87] that generate a current in the passive circuit by coupling it to another one (the drive) that is voltage biased. Differently from extended samples, that rely on momentum exchange [88], the mesoscopic drag is based on the exchange of energy. This has been emphasized in proposals of thermal drag currents where only heat flows

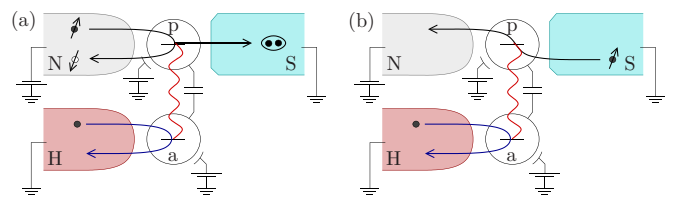


FIG. 1. Hybrid normal-superconductor heat engine based on coupled quantum dots (p , for passive and a , for active). Heat injected from the hot reservoir (H) induces the transfer of either (a) a Cooper pair in the superconductor (S) via an Andreev reflection in the normal lead (N), or (b) a quasiparticle transferred between S and N. In both cases, an electric current is generated in the passive subsystem.

in the drive system [89–98] and of absorption refrigerators [99]. In a recent work [100], we found that the interplay of charge fluctuations and Andreev reflection processes gives rise to a drag current when the passive system contains a superconducting electrode. These processes compete with a second mechanism due to single quasiparticle tunneling. Here we explore how these mechanisms can make the system work as a nonlocal thermoelectric heat engine. For this purpose, we consider a hybrid three-terminal configuration consisting of two Coulomb-coupled quantum dots (*a*, for active and *p*, for passive), as sketched in Fig. 1. The active dot is coupled to a hot normal terminal (H). The passive one is connected to one normal (N) and one superconducting (S) terminals, see Refs. [101–103] for discussions of related experimental implementations. We analyze the regimes where the generated current is mediated by the two mentioned mechanisms [Andreev reflection, cf. Fig. 1(a), and correlated quasiparticles filtered by the superconducting density of states, cf. Fig. 1(b)]. They are shown to give opposite contributions, which in the intermediate regime where the two processes coexist reduces the thermoelectric performance of the engine (in terms of the generated power and efficiency).

Additionally it is interesting to explore the properties of the heat currents, which may make the device work as a refrigerator (when heat is extracted from the coldest reservoir) or as a heat pump (when heat flows into the hottest one). Multitask operations in three terminal conductors have been recently identified [104] where combinations of two or more such operations are met, see also Refs. [105,106].

The remainder of the manuscript is organized as follows. The system and the model are described in Sec. II. The limiting regimes where Andreev and quasiparticle transport dominate are discussed in Secs. III and IV, respectively, by using a master equation approach [107,108] that provides a physical understanding of the involved mechanisms. The two regimes require different master equations which will be discussed separately. The intermediate regime is explored numerically in Sec. V by invoking a nonequilibrium Green's functions technique [109]. Finally, conclusions are presented in Sec. VI.

II. HYBRID COUPLED QUANTUM DOT SYSTEM

A. Hamiltonian

We aim at the simplest description of the main mechanisms involved in the passive current generation. Spin is essential for pairing in the passive system. In the active dot, only charge fluctuations are required in order to generate a passive current [86]. Therefore, we ignore the spin degree of freedom and intradot Coulomb interactions in the active system for simplicity. This provides a good description of transport (up to spin degeneracy prefactors) as long as double occupancy of the active dot is negligible and in the absence of interdot spin-spin interactions. Note however that intradot Coulomb interactions in the passive dot do affect the pairing processes and need to be taken into account.

Our system is hence described with the Hamiltonian

$$\mathcal{H} = \mathcal{H}_l + \mathcal{H}_{\text{dqd}} + \mathcal{H}_t. \quad (1)$$

The first term is the Hamiltonian for the reservoirs,

$$\begin{aligned} \mathcal{H}_l = & \sum_{k,\sigma} \varepsilon_{k,S} \hat{c}_{k,S,\sigma}^\dagger \hat{c}_{k,S,\sigma} + \sum_k \Delta (\hat{c}_{k,S,\uparrow}^\dagger \hat{c}_{k,S,\downarrow}^\dagger + \text{h.c.}) \\ & + \sum_k \varepsilon_{k,H} \hat{c}_{k,H}^\dagger \hat{c}_{k,H} + \sum_{k,\sigma} \varepsilon_{k,N} \hat{c}_{k,N,\sigma}^\dagger \hat{c}_{k,N,\sigma}, \end{aligned} \quad (2)$$

where $\hat{c}_{k,\beta,\sigma}$ is the annihilation operator for electrons with energy ε_k , momentum k and spin $\sigma = \{\uparrow, \downarrow\}$ in terminal $\beta = \text{H,N,S}$ (note that for $\beta = \text{H}$ we drop the spin index), and Δ is the order parameter in the superconducting electrode. Each of the metallic reservoirs is in local thermodynamic equilibrium with electrochemical potential μ_β and temperature T_β . The superconducting chemical potential μ_S sets the common Fermi energy, which we take from now on as the reference energy, $\mu_S = 0$. The passive subsystem is held at a lower temperature ($T \equiv T_N = T_S$) than that of the active subsystem ($T < T_H$).

The second term in Eq. (1) accounts for the double quantum dot,

$$\mathcal{H}_{\text{dqd}} = \sum_\alpha \varepsilon_\alpha \hat{n}_\alpha + U_p \hat{n}_{p,\uparrow} \hat{n}_{p,\downarrow} + U_{ap} \hat{n}_a \hat{n}_p, \quad (3)$$

where the number operators are defined as $\hat{n}_p = \sum_\sigma \hat{n}_{p,\sigma} = \sum_\sigma \hat{d}_{p,\sigma}^\dagger \hat{d}_{p,\sigma}$ for the passive dot, and $\hat{n}_a = \hat{d}_a^\dagger \hat{d}_a$ for the active one. Here, $\hat{d}_{p,\sigma}$ and \hat{d}_a denote electron annihilation operators and ε_α are the dot energy levels. The interdot charging energy is U_{ap} , and U_p is the (intradot) charging energy of the passive dot. The coupling between the dots and the leads is given by the term

$$\begin{aligned} \mathcal{H}_t = & \sum_{k,\sigma} (t_N \hat{d}_{p,\sigma}^\dagger \hat{c}_{k,N,\sigma} + t_S \hat{d}_{p,\sigma}^\dagger \hat{c}_{k,S,\sigma} + \text{h.c.}) \\ & + \sum_k (t_H \hat{d}_a^\dagger \hat{c}_{k,H} + \text{h.c.}), \end{aligned} \quad (4)$$

where the t_β are the dot-lead tunnel couplings. In the following, we consider the wide-band approximation, in which case the tunnel hybridization strength is given by $\Gamma_\beta = 2\pi |t_\beta|^2 \rho_0^\beta$, where ρ_0^β is the corresponding electrode's density of states in its normal state.

B. Power and efficiency

Let J_β be the heat flux and I_β the charge current in terminal β . While charge conservation ensures $I \equiv I_N = -I_S$ and $I_H = 0$, energy conservation in the conductor is only expressed as $J_N + J_S = P - J_H$, where

$$P = -VI \quad (5)$$

is the power dissipated (Joule heating) by a charge flowing in favor of a voltage bias $V = (\mu_N - \mu_S)/e$. In that case, $P < 0$.

In the absence of additional forces ($V = 0$), the difference $T_H - T > 0$ causes heat to be transferred from the active to the passive dot via the Coulomb coupling U_{ap} [34]. A nonlocal thermoelectric engine is able to convert this injected heat flow into a charge current generated in the passive subsystem. Then, a finite voltage V can be applied to counteract I . In the range of V such that P is positive, work can be done against an external load. The ratio between the output power in the

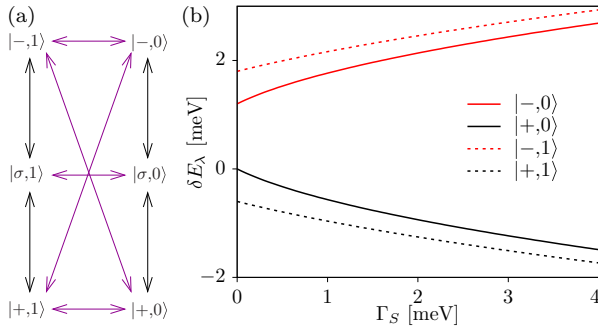


FIG. 2. (a) Eigenstates of the proximitized quantum dot. The arrows represent the different transitions due to tunneling in the passive (black) and active systems (purple arrows). Note that the latest cannot change the parity of the passive system. (b) Separation of the even and odd states, $\delta E_{\pm,n} \equiv E_{\pm,n} - E_{\sigma,n}$, as a function of the pairing, Γ_S , with $U_p = 2U_{ap} = 1.2$ meV and $\varepsilon_a = 0$.

passive circuit and the heat absorbed from the active one,

$$\eta = \frac{P}{J_H} \quad (6)$$

is the thermodynamic efficiency of the engine, which is limited by the Carnot bound, $\eta \leq \eta_C = 1 - T/T_H$ [1]. For voltages larger than the stall voltage (a non-local analog of the thermovoltage, where the thermoelectric current is compensated by electrons flowing in favor of the bias), power is dissipated and the engine stops working. It is then necessary to calculate P , J_H and η to fully describe the heat engine properties of our device.

Sign changes of the heat currents define the other thermodynamic operations. When positive, J_N and J_S will characterise the cooling power of the system working as a refrigerator of the corresponding reservoir. A heat pump occurs when $J_H < 0$.

III. ANDREEV REGIME

When the superconducting gap Δ is the largest energy scale of the problem, one can replace the superconductor and its coupling to the passive dot with a pairing term in Eq. (3):

$$\mathcal{H}_{\text{dqd}} \rightarrow \mathcal{H}_{\text{dqd}} + \Gamma_S (\hat{d}_{p,\uparrow}^\dagger \hat{d}_{p,\downarrow}^\dagger + \text{h.c.}), \quad (7)$$

see e.g., Refs. [110–112] for microscopic justifications of this approximation. Then, \mathcal{H}_{dqd} can be exactly diagonalized yielding the eigenenergies

$$E_{\sigma,n} = \varepsilon_p + n(\varepsilon_a + U_{ap}), \quad (8)$$

$$E_{\pm,n} = n\varepsilon_a + A_{\mp,n}, \quad (9)$$

with the associated eigenstates

$$\{|\sigma, n\rangle, |\pm, n\rangle = \mathcal{N}_{\pm,n}^{-1} (A_{\pm,n}|0, n\rangle - \Gamma_S|2, n\rangle)\}, \quad (10)$$

represented in Fig. 2(a). Here, $n = 0, 1$ keeps record of the charge number in the active dot and we have defined

$$A_{\pm,n} = \tilde{\varepsilon}_n \pm \sqrt{(\tilde{\varepsilon}_n)^2 + \Gamma_S^2}, \quad (11)$$

with $\tilde{\varepsilon}_n = \varepsilon_p + U_p/2 + nU_{ap}$. The states in the proximitized dot are expressed in terms of the charge basis $\{0, \sigma, 2\}$ and

fall into either the odd ($|\sigma\rangle$) or the even ($|\pm\rangle$) charge sector. The latter are important because they involve coherent superpositions of states with 0 or 2 electrons, and consequently contribute to the transfer of Cooper pairs through the dot.

For small lead-dot couplings, a master equation approach correctly describes the system dynamics in terms of sequential transitions between the different states, as sketched in Fig. 2(a). We get the stationary occupation of the different states, P_λ , by solving the set of equations

$$\sum_{\alpha\beta\kappa} (W_{\lambda\kappa}^{\alpha\beta} P_\kappa - W_{\kappa\lambda}^{\alpha\beta} P_\lambda) = 0. \quad (12)$$

The rates $W_{\lambda\kappa}^{\alpha\beta} = \Gamma_{\lambda\kappa}^{\alpha\beta} + \gamma_{\lambda\kappa}^{\alpha\beta}$ for the transition $|\kappa\rangle \rightarrow |\lambda\rangle$ due to the tunneling of an electron from (to) lead β in (out of) dot α are given, respectively, by

$$\Gamma_{\lambda\kappa}^{\alpha\beta} = \Gamma_\beta |\langle \lambda | \hat{\delta}_\alpha^\dagger | \kappa \rangle|^2 f_\beta(E_\lambda - E_\kappa) \quad (13)$$

$$\gamma_{\lambda\kappa}^{\alpha\beta} = \Gamma_\beta |\langle \lambda | \hat{\delta}_\alpha | \kappa \rangle|^2 [1 - f_\beta(E_\kappa - E_\lambda)], \quad (14)$$

where $f_\beta(E) = \{1 + \exp[(E - \mu_\beta)/k_B T_\beta]\}^{-1}$ is the Fermi function. The operator $\hat{\delta}_\alpha$ annihilates an electron in dot α i.e., $\hat{\delta}_\alpha = \hat{d}_\alpha$ and $\hat{\delta}_p = \sum_\sigma \hat{d}_{p\sigma}$. These rates allow us to determine both the charge current,

$$I = e \sum_{\lambda,\kappa} (\gamma_{\lambda\kappa}^{pN} - \Gamma_{\lambda\kappa}^{pN}) P_\kappa, \quad (15)$$

and the heat flux out of terminal β ,

$$J_\beta = \sum_{\lambda,\kappa} (E_\lambda - E_\kappa - \mu_\beta) (\gamma_{\kappa\lambda}^{\alpha\beta} P_\lambda - \Gamma_{\lambda\kappa}^{\alpha\beta} P_\kappa). \quad (16)$$

The transitions between odd and even parity states can be both due to an electron or to a hole tunneling process. The relative rate at which one or the other process contributes more depends on the ratio $A_{\pm,n}/\Gamma_S$ that dictates the asymmetry of the even superpositions in Eq. (10). It depends on the energy of the passive dot and, in particular, on the occupation of the active one, n . In fact, the gap between even and odd states is itself a function of n , as shown in Fig. 2(b). Hence, fluctuations of the charge in the active dot change the contribution of electron- or holelike processes in the passive dot in a dynamical way. This results in a rectification effect that leads to a finite I at $V = 0$.

In Fig. 3 we plot the thermoelectric current in the passive circuit as a function of the energies of the two dot levels, which can be shifted with external gate voltages [113]. A finite current is generated in the passive circuit due to Coulomb interactions with the hotter active circuit. Similarly to Ref. [100], the passive system response occurs around the center of the stability diagram, where fluctuations of the charge of both dots are enhanced. However, while the drag current in Ref. [100] is driven by nonequilibrium fluctuations created by a dc bias applied across the active dot, the generated current here is driven by purely thermal means.

For small coupling to the S electrode, the current changes sign by tuning ε_p , see Fig. 3(a). The current direction is determined by the character (electron- or holelike) of the dominant transitions, which is strongly dependent on the position of the passive dot energy. The generated current can be seen at a much wider range of gate voltages when Γ_S is further

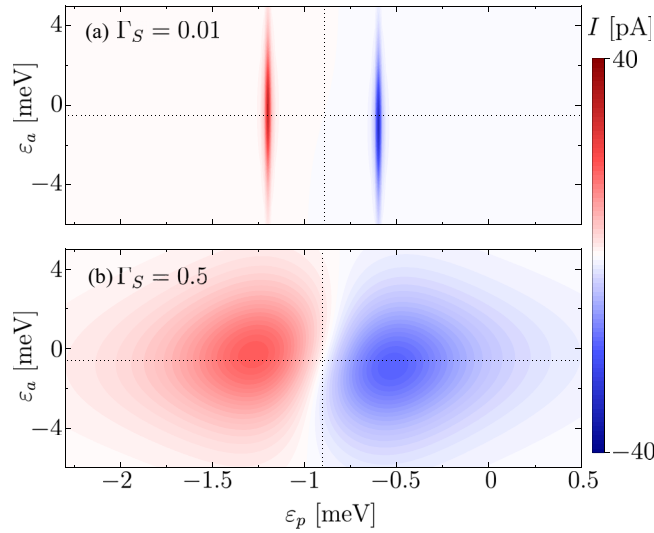


FIG. 3. Charge current in the passive subsystem as a function of active and passive dot levels for (a) $\Gamma_S = 0.01$ meV and (b) $\Gamma_S = 0.5$ meV. Parameters (in meV): $k_B T_H = 1.5$, $k_B T_C = 1$, $\Gamma_H = \Gamma_N = 0.01$, $U_{ap} = 0.6$, $U_p = 1.2$ and $V = 0$.

increased, see Fig. 3(b). An important aspect is that the generated current changes sign in this case also when tuning the level position of the active dot, keeping ε_p fixed, as can be seen in Fig. 4(a). This way, both the magnitude and the sign of the passive current can be controlled by using the parameters of the active system as an external knob. Line cuts of the currents along the dotted lines in Fig. 3 are plotted in Figs. 4(a) and 4(b) for clarity.

Let us now investigate the heat currents. To make a comparison, we show in Figs. 4(c) and 4(d) the heat current $J_H =$

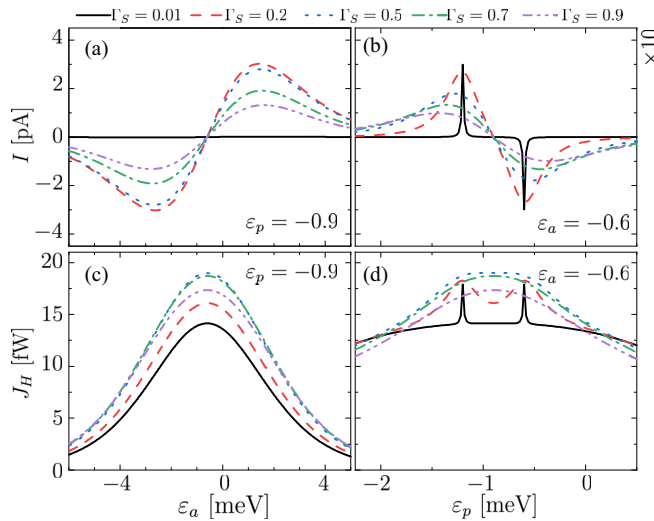


FIG. 4. (a), (b) Zero bias charge and (c), (d) heat current from H for different couplings to the superconductor: $\Gamma_S = 0.01, 0.2, 0.5, 0.7$, and $\Gamma_S = 0.9$ meV. The different panels show the dependence of the currents as a function of both the active (a), (c) and passive (b), (d) dot levels, along the dashed lines in Figs. 3(a) and 3(b). The current in panel (b) is divided by 10 to fit with the axis of panel (a). Other parameters are as in Fig. 3.

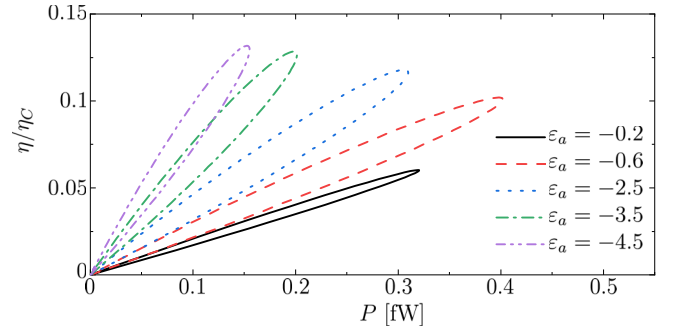


FIG. 5. Thermoelectric performance of the heat engine in the Andreev regime for different values of ε_a . Power and efficiency are computed for voltages ranging between zero and the stall voltage, where $P = \eta = 0$. Other parameters are as in Fig. 3(a).

$-J_N$ together with the charge current through the passive dot. While I has the characteristic sign changes discussed above, J_β does not change sign, as expected for heat between a hot and a cold reservoir in the absence of external work done on the system. This energy is transferred through the interdot repulsion U_{ap} into the passive subsystem in the region where the charge states of the two quantum dots fluctuate strongly. We recall that in the infinite gap approximation the superconducting reservoir is only treated as a source of pair correlations for the p dot and therefore we have two heat fluxes only. In the next sections, we will relax this approximation and study also the heat that flows in the superconductor.

Furthermore, the charge and heat currents in Fig. 4 show a nonmonotonic behavior of the maximal charge current with the coupling to the superconductor: for small values of Γ_S , the generated current increases with the coupling to S, as expected. However, as it becomes comparable to and larger than the charging energy, both I and J_H get reduced. This is understood in terms of the increased splitting between the even and odd parity states, see Fig. 2(b). For large Γ_S , the fluctuations between the lowest energy $|+, n\rangle$ state and the $|\sigma, n\rangle$ states (due to either the tunneling of an electron or a hole) are hence suppressed, as soon as $E_{\sigma, n} - E_{+, n} > k_B T$, in a similar way as the charging energy suppresses single-electron transport [114]. These fluctuations are necessary both for the charge and the heat currents, resulting in a backaction on the thermal transport between H and N. Hence, pairing cooperates with U_{ap} in blocking the current. Differently from Coulomb blockade, this pairing blockade effect is quantum coherent.

We are now in a position to assess the thermoelectric efficiency η . Positive power P is produced when the current flows against the applied voltage V . This occurs between $V = 0$ and the stall voltage where the bias compensates the thermoelectric current (making $I = 0$). Thus, in our efficiency calculations we select the maximum negative current, which occurs around $\varepsilon_p = -(U_p + U_{ap})/2 + U_{ap}/2$, as shown in Fig. 4. By tuning V , we calculate both P and η , which both vanish at $V = 0$ and at the corresponding stall voltage where $I = 0$, see Eqs. (5) and (6), as shown in Fig. 5. We observe that power and efficiency are optimized for different values of ε_a . When the gates are such that current is maximal (around $\varepsilon_a = -0.6$ meV), the power is enhanced. However, the effi-

ciency increases when both ε_a and $\varepsilon_a + U_{ap}$ go well below μ_H , at the expense of reducing the fluctuations and hence the generated power. In order to have a sizable performance, the value of Γ_S needs to be optimized as well. We need it to be of the order of $A_{\pm,n}$ in order to maximize the effect of the fluctuations of the pairing wave function. In the limits where either $\Gamma_S \gg \tilde{\varepsilon}_n$ or the opposite, the asymmetry between electron- and holelike processes disappears and thereby the thermoelectric effect vanishes.

IV. QUASIPARTICLE REGIME

The other contribution to transport is due to quasiparticles. They are expected to dominate in different configurations: either when the passive dot level is close to the superconducting gap, when $\Gamma_S \rightarrow 0$, or at high temperatures. In these cases, tunneling of Cooper pairs is strongly suppressed. In order to discriminate its contribution, we consider a simple model where the effect of the superconductor is only due to its density of states (DoS). The spin of the electron does not play a crucial role, so for simplicity we assume the limit $U_p \gg k_B T$ where a charge basis captures the main effect.

We are then left with four states $|n_p, n_a\rangle$, with 0 or 1 electron in the passive and active dots. The hopping rates in the passive subsystem are

$$\Gamma_{1n,0n}^{p,\beta} = \Gamma_{\beta} v_{\beta n} f_{\beta n} \quad \text{and} \quad \gamma_{0n,1n}^{p,\beta} = \Gamma_{\beta} v_{\beta n} (1 - f_{\beta n}), \quad (17)$$

where $v_{Nn} = 1$, and v_{Sn} is the normalized superconductor DoS. Notably, we take into account the dependence on the active dot occupation $n = 0, 1$ via the Coulomb repulsion strength U_{ap} . This is better seen in the Fermi functions as $f_{\beta n} = f_{\beta}(nU_{ap} + \varepsilon_p)$ for $\beta = N, S$. We model the superconductor DoS with the Dynes form [115],

$$v_{Sn} = \left| \text{Re} \frac{\varepsilon_p + nU_{ap} + i\chi}{\sqrt{(\varepsilon_p + nU_{ap} + i\chi)^2 - \Delta^2}} \right|, \quad (18)$$

where χ takes into account quasiparticle occupation in the gap. The rates in the active dot read

$$\Gamma_{n1,n0}^{a,H} = \Gamma_H f_{Hn} \quad \text{and} \quad \gamma_{n0,n1}^{a,H} = \Gamma_H (1 - f_{Hn}), \quad (19)$$

where $f_{Hn} = f_H(nU_{ap} + \varepsilon_a)$. We can find the stationary occupation probabilities P_{n_p, n_a} by solving the system of equations (12). With these, we again calculate charge and heat currents using Eqs. (15) and (16).

It was shown in Ref. [34] (and later confirmed experimentally [36]) that a similar configuration (based there on all-normal reservoirs) leads to a nonlocal thermoelectric response provided the tunneling rates in the passive system are energy-dependent and left-right asymmetric. In our hybrid configuration, this property is enabled by the superconducting DoS: tunneling is suppressed at energies $\varepsilon_p + nU_{ap}$ within the gap, and enhanced at energies close to the coherence peaks, as sketched in Fig. 6 for two different level positions. It can be shown that in the case where the tunneling couplings Γ_{β} are energy independent, a zero-bias current

$$I(V=0) \propto (v_{S0} - v_{S1})(f_{N0} - f_{N1}) \quad (20)$$

is generated [100]. This current is shown in Fig. 7(a). As expected, $I = 0$ when both energies ε_p and $\varepsilon_p + nU_{ap}$ lie in the gap

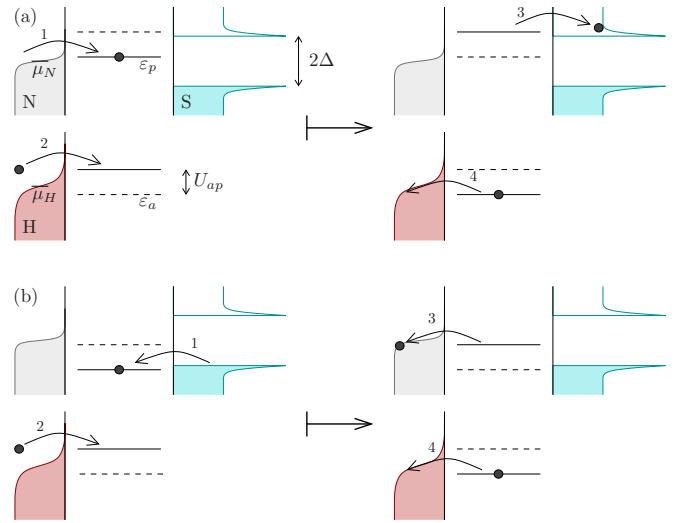


FIG. 6. Quasiparticle transport enabling sequences at zero bias. A finite current is induced by a temperature difference $T_H > T_N = T_S$ whose sign depends on the passive dot energy. Charge flows (a) from N to S for $\varepsilon_p - \mu_N \in (\Delta - U_{ap}, \Delta)$, and (b) in the opposite direction when $\varepsilon_p - \mu_N \in (-\Delta - U_{ap}, -\Delta)$. The order of the tunneling events is indicated.

[region with $\varepsilon_p - \mu_N \in (-\Delta, \Delta - U_{ap})$, marked as C]. The conditions for transport appear in regions of width given by the Coulomb repulsion U_{ap} , marked as B [with $\varepsilon_p - \mu_N \in (-\Delta - U_{ap}, -\Delta)$] and D [with $\varepsilon_p - \mu_N \in (\Delta - U_{ap}, \Delta)$] in Fig. 7(a). There, electrons/holes around the Fermi energy in N (such that $v_{S0} = 0$ at those energies) can exchange energy with the passive dot and be transferred over/below the gap

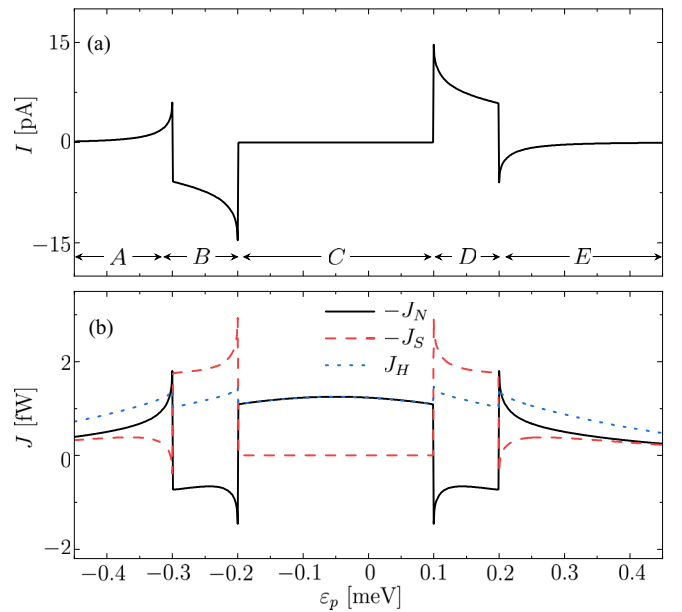


FIG. 7. Zero bias (a) charge and (b) heat currents in the different terminals in the quasiparticle regime. They are plotted as functions of the passive dot energy. Parameters: $\Delta = 0.2$ meV, $k_B T_H = 0.3$ meV, $k_B T = 0.2$ meV, $U_{ap} = 0.1$ meV, $\varepsilon_a = -U_{ap}/2$, $\Gamma_H = \Gamma_N = \Gamma_S = 0.01$ meV, and $\chi = 10^{-6}$.

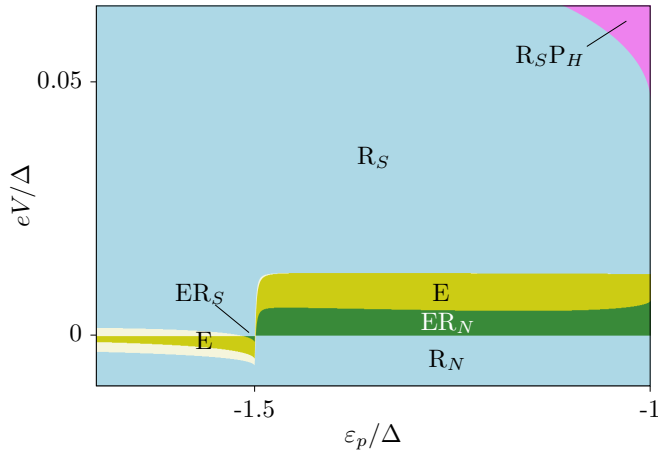


FIG. 8. Map of the different thermal operations as a function of the passive dot energy and the applied voltage. Different colors mark different thermodynamic operations, as indicated (white means no useful operation). They are labeled with E, when the system works as a heat engine, and with R_α and P_α , when it works as a refrigerator or a heat pump in terminal α . Parameters: $k_B T = \Delta$, $k_B T_H = 1.1\Delta$, $\varepsilon_a = -0.3\Delta$, $\chi = 10^{-4}$. Other parameters as in Fig. 7.

(when $\nu_{S1} \neq 0$). In this configuration, the charge current is antisymmetric around $\varepsilon_p = -U_{ap}/2$. Note that the change of sign around the particle-hole symmetry point is opposite to the one obtained in the Andreev regime discussed in Sec. III. Also differently from that case, the charge current does not change sign with the position of the active dot, due to the lack of coherence in the passive dot.

The same transport windows are evident in the heat transport, as shown in Fig. 7(b). In region C, where transport in terminal S is avoided by the gap, all the heat injected from H is absorbed by the normal contact. Out of this region, the heat current sign gives insights of the relevant mechanism for the generated current. In region B electrons below the gap in S enter the passive dot when the active one is empty and tunnel out below the chemical potential of N once the active dot has been occupied. This way, $I < 0$, the superconductor is heated up ($J_S < 0$) and the normal contact is refrigerated ($J_N > 0$), as sketched in Fig. 6(b). In the opposite region D, electrons tunnel from over μ_N into the passive dot, with an empty active dot, and tunnel out over the superconducting gap after gaining an energy U_{ap} from the interaction with an electron having occupied the passive dot, see Fig. 6(a). In this case, while the charge flows in the opposite direction, $I > 0$, one still finds $J_S < 0$ and $J_N > 0$, as expected. Noticeably, we find that close to $\varepsilon_p - \mu_N \approx \pm(\Delta + U_{ap})$ (in the frontiers of A-B and D-E regions), the peaks of the superconducting DoS enable an additional change of sign in the charge current that cools the superconductor. In all these cases (except for region C), the system works as a hybrid thermal engine [104] capable of simultaneously generate power and cool (either terminal N or S) from a single resource (heat in reservoir H). This possibility is further explored in Fig. 8 in the presence of a finite voltage. This way, we find an additional hybrid operation where high enough voltages are able to reverse the heat current J_H , while $J_S > 0$ (violet region in Fig. 8, labeled as $R_S P_H$). Hence, the system works both as a refrigerator of S and a heat pump

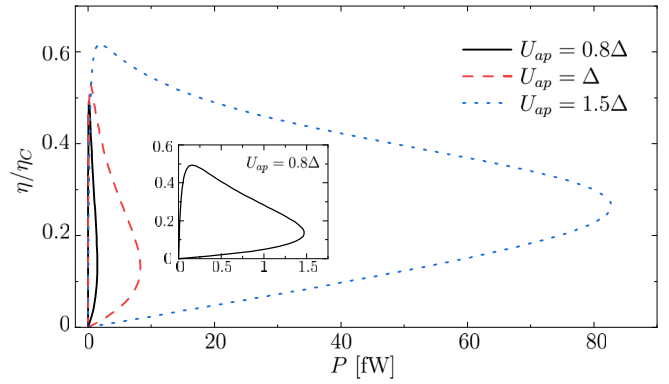


FIG. 9. Thermoelectric efficiency in the quasiparticle regime, for different interaction U_{ap} . Each point is optimized with respect to the value of ε_p . The inset zooms the curve for $U_{ap} = 0.8\Delta$ in, for clarity. Other parameters as in Fig. 7.

into the hottest reservoir, H. Tuning the voltage facilitates the cooling of the N or S terminals (light blue regions in Fig. 8), very much like a usual quantum dot Peltier refrigerator [116,117]. Here these operations are affected by the coupling to the other dot. The configuration map in Fig. 8 is repeated by inverting over the $V = 0$ and $\varepsilon_p - \mu_N = -U_{ap}/2$.

The asymmetric filtering of some electronic tunneling events, here facilitated by the superconducting DoS, is expected to enable optimal heat to power conversion in terms of power and efficiency [34]. Consider for instance region D, and the scheme in Fig. 6(a): the gap avoids the electron tunneling from N to subsequently tunnel to S without having exchanged an energy U_{ap} with the active system. Once this is done, the coherence peak makes it more favorable to tunnel to S than back to N. This way, most of the cycles for which an amount of energy U_{ap} is transferred from the active to the passive system result in an electron being transferred from N to S. This is confirmed in Fig. 9, where power increases by two orders of magnitude with respect to the Andreev regime, with the efficiency being doubled. Furthermore, for low T , high efficiencies approaching η_C are obtained at low power (but still one order of magnitude larger) by taking advantage of the Bardeen-Cooper-Schrieffer peak. The maximal efficiency is hence limited by the sharpness of the coherence peak, which is affected by the Dynes parameter, χ . In this case, the thermoelectric performance improves when increasing U_{ap} , such that electrons gain enough energy from H to overcome the gap. Increasing temperature smears the effect of the spectral features and hence affects the performance.

V. INTERMEDIATE REGIME

In this section we explore the thermoelectric performance of the engine in the intermediate regime where the temperature is low and the superconducting energy gap Δ is comparable to other energy scales. Then it is important to take into account the contributions from both Andreev and quasiparticle transport mechanisms in the calculations. This is possible by employing the non-equilibrium Green's functions (NEGF) technique [100], which furthermore takes the finite linewidth of the quantum dot states (which is neglected in the

sequential tunneling master equations discussed in previous sections) into account.

Within this formalism, the different currents through terminal $\beta = N, S, H$, can be calculated by using

$$I_\beta = \frac{e}{2\hbar} \int \frac{d\omega}{2\pi} \text{Tr}(\hat{\sigma}_z \mathcal{I}_\beta), \quad (21)$$

$$J_\beta = \frac{1}{2\hbar} \int \frac{d\omega}{2\pi} \text{Tr}[(\omega I_2 - eV_\beta \hat{\sigma}_z) \mathcal{I}_\beta], \quad (22)$$

for charge and heat, respectively, with

$$\begin{aligned} \mathcal{I}_\beta = & G_\alpha^R(\omega) \Sigma_{\alpha,\beta}^<(\omega) + G_\alpha^<(\omega) \Sigma_{\alpha,\beta}^A(\omega) \\ & - \Sigma_{\alpha,\beta}^R(\omega) G_\alpha^<(\omega) - \Sigma_{\alpha,\beta}^<(\omega) G_\alpha^A(\omega). \end{aligned} \quad (23)$$

Here the terminal index β fixes the index $\alpha = p, a$ of the quantum dot coupled to it, and I_2 and $\hat{\sigma}_i$ are the 2×2 identity and Pauli matrices, respectively. The retarded and lesser self-energies are given by $\Sigma_{a,H}^R(\omega) = -i\Gamma_{a,H}$, $\Sigma_{p,N}^R(\omega) = -i\Gamma_{p,N}I_2$, and $\Sigma_{p,S}^R(\omega) = -i\Gamma_S b(\omega)(I_2 - \Delta\omega^{-1}\hat{\sigma}_x)$, where $b(\omega) \equiv |\omega|(\omega^2 - \Delta^2)^{-1/2}\theta(|\omega| - \Delta) - i\omega(\Delta^2 - \omega^2)^{-1/2}\theta(\Delta - |\omega|)$, with the Heaviside step function, $\theta(E)$, and $\Sigma_{\alpha,\beta}^<(\omega) = -2i\text{Im}(\Sigma_{\alpha,\beta}^R)f_\beta(\omega)$. The interacting retarded and lesser components of the Keldysh Green's function of dot α , $G_\alpha^{R/<}$, are calculated self-consistently by using the Dyson and the Keldysh equations

$$G_\alpha^R = \left\{ [g_\alpha^R]^{-1} - \Sigma_{\alpha,\text{int}}^R \right\}^{-1}, \quad (24)$$

$$G_\alpha^< = G_\alpha^R (\Sigma_{\alpha,\text{leads}}^< + \Sigma_{\alpha,\text{int}}^<) G_\alpha^A, \quad (25)$$

where g_α^R is the noninteracting retarded Green's function of dot α , and $\Sigma_{\alpha,\text{int}}$ is the corresponding interaction selfenergy of the dot α due to its Coulomb interaction with other charges in the dots. We refer the interested reader to the Supplemental Material in Ref. [100] for the explicit expressions of these self-energies and Green's functions and also for the details of the numerical procedure used to solve the above equations selfconsistently. Here we chose the parameters such that the system falls in the intermediate regime where both Andreev and quasiparticle mechanisms contribute. In particular, their relative contribution is controlled by the coupling Γ_S .

As we learned in the previous sections, the contribution of the two different mechanisms (Cooper pair and quasiparticle dominated transport) depends strongly on the position of the quantum dot levels. The Andreev (pairing) induced current is finite around the particle-hole symmetry point, see Fig. 3. Differently, the quasiparticle contribution occurs close to the gap borders, see Fig. 7. Hence, their competition results in a rich behavior of the current generated at $V = 0$. This is shown in Fig. 10(a): in the center of the stability diagram the Andreev contribution dominates, with the current sign being as predicted by the rate equation description in Sec. III. As the passive dot level deviates from this region, the quasiparticle contribution starts to dominate and the current changes sign, in agreement with the results in Sec. IV. Importantly, for fixed values of ε_p , the charge current changes sign as a function of ε_a . This effect was found in the Andreev regime, cf. Figs. 3(b) and 4(a), and is hence a signature of quantum coherence persisting in the intermediate regime. This is interesting since it allows us to control the generated current by only using the

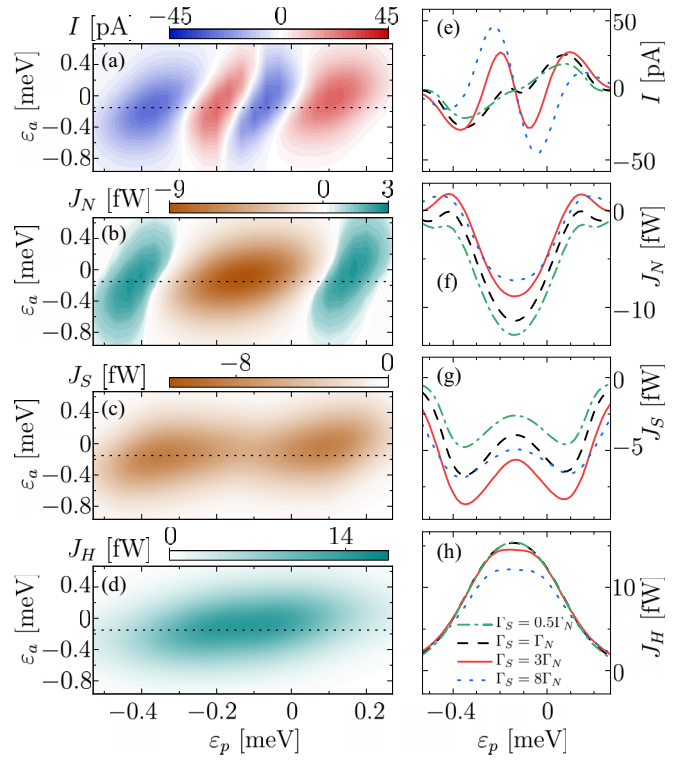


FIG. 10. (a)–(d) Charge I and heat currents J_N , J_S and J_H as functions of the active and passive dot energies for $\Gamma_S = 3\Gamma_N$. (e)–(h) Line cuts of left panels at $\varepsilon_a = -(U_{ap} + U_p)/2 = -0.15$ meV (indicated by dashed lines in left panels) and for different values of $\Gamma_S = 0.5\Gamma_N$, Γ_N , $3\Gamma_N$ and $8\Gamma_N$. Other parameters are $\Delta = 0.2$ meV, $k_B T_H = 2k_B T = 0.2$ meV, $\Gamma_H = \Gamma_N = 0.01$ meV, $U_p = 1.6U_{ap} = 0.16$ meV and $V = 0$.

active dot parameters: T_H generates the current and ε_a controls its direction.

The different contributions are also visible in the heat currents, plotted in Figs. 10(b)–10(d). As expected, the heat current injected from H is always positive (for $V = 0$). It is restricted to the region where charge fluctuations in both dots are present [70], see Fig. 10(d), emphasizing the role of electron-electron interaction in the heat exchange between the systems. The latter occurs as well in the passive system currents, with two particular aspects to point out: heat always flows into the superconductor ($J_S < 0$) but is slightly suppressed by the gap for ε_p close to the particle-hole symmetry point. Most interestingly, J_N changes sign at the crossover between the Andreev and the quasiparticle regimes, leading to cooling, see Fig. 10(b). Hence, we recover the ER_N operation shown in Fig. 8 as soon as a small voltage V is applied.

The relative contribution of the two mechanisms depends strongly on the parameters. Crucially, it depends on the coupling to the superconductor, because the Andreev reflection is suppressed for low Γ_S . This is shown in Figs. 10(e)–10(h), where cuts of the left-column panels at $\varepsilon_a = -(U_{ap} + U_p)/2$ (marked by dotted lines) are plotted for different Γ_S . Remarkably, Fig. 10(e) shows how the Andreev contribution to the charge current dominates for large Γ_S and totally disappears for sufficiently small couplings. Note that the quasiparticle contribution gets correspondingly reduced but can still be

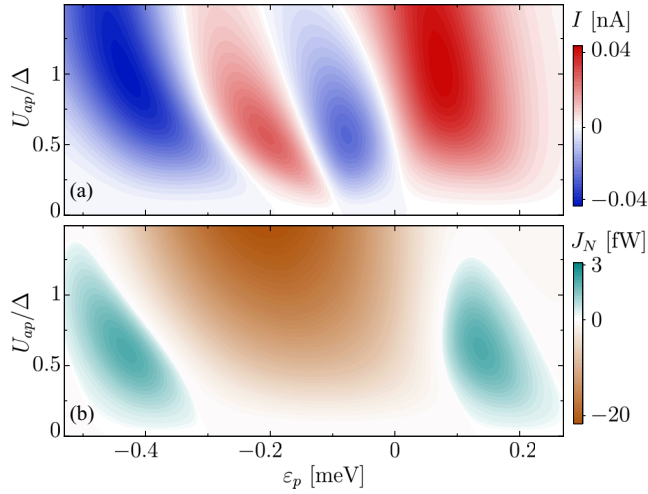


FIG. 11. (a) Charge current, I , and (b) heat current, J_N , as functions of the interdot Coulomb interaction strength U_{ap} and the passive dot energy for $\Gamma_S = 3\Gamma_N$. $\varepsilon_a = -0.15$ meV and other parameters are as in Fig. 10.

visible for large Γ_S by the effect of the gap border. In this case, the sharp features in Fig. 7 due to the gap are smeared here due to the finite level-width of the passive dot. We observe a different behavior in Fig. 10(f), where the contribution of the strong gap features to the cooling of N are favored by increasing the coupling to the superconductor. While J_S gets strongly reduced for low Γ_S , cf. Fig. 10(g), the injected current from the hot bath is barely unaffected, except for large couplings, see Fig. 10(h). The latter can be attributed to the pairing blockade effect introduced in Sec. III. Note, however, a stronger nonmonotonic behavior of J_S in Fig. 10(g), that is caused by the increasing role at high Γ_S of pair tunneling, which does not carry heat.

The interplay of the two processes furthermore depends on the interaction between the two quantum dots, U_{ap} . This is shown in Fig. 11. The quasiparticle contribution to the charge current is maximal when $U_{ap} \lesssim \Delta$ i.e., when quasiparticles gain/lose enough energy from the interaction with the active dot to overcome the gap, see Fig. 11(a). For the same reason, the cooling of terminal N, due to quasiparticles, is suppressed for $U_{ap} > \Delta$, see Fig. 11(b). The Andreev contribution is on the contrary reduced by the interaction, as it reduces the hybridization of the even parity states (essential for the current generation via pairing) when it becomes large compared to Γ_S , see Eq. (10). For large U_{ap} , the Andreev contribution is washed out by quasiparticles, as expected.

The generated current leads to useful power in the presence of a finite bias voltage. This affects the properties of the heat currents as well. In Fig. 12 we show the generated power and the heat current in N. Figures 12(a) and 12(b) show the low voltage behavior, with line cuts for fixed V plotted in Figs. 12(c)–12(f). In the low (but positive) voltage regime, finite power is generated in two regions as we tune ε_p , which correspond to the quasiparticle and Andreev dominated regimes. The quasiparticle dominated region (around $\varepsilon_p \approx -0.4$ meV) results in larger power and larger stall voltages for this intermediate configuration. The cooling of terminal N

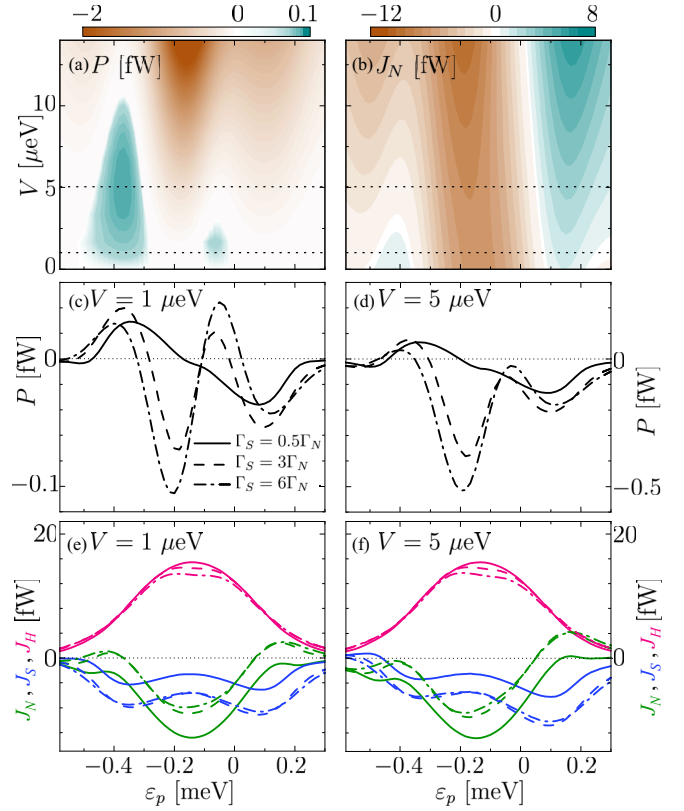


FIG. 12. (a) Power and (b) normal terminal heat current in the low voltage regime as functions of voltage and the passive dot energy. (c)–(f) show line cuts of the power and the different heat currents for different Γ_S and two different voltages indicated by dotted lines in (a) and (b). Same parameters as in Fig. 10, with $\varepsilon_a = -0.15$ meV.

discussed above coexists with the power production, though the limiting voltage for having $J_N > 0$ is smaller than the stall voltage for $P > 0$, compare Figs. 12(a) and 12(b). This is consistent with the behavior shown in Fig. 8, where the E and ER_N are adjacent for quasiparticle induced transport. For the configuration chosen here, the efficiency is reduced to $\eta \approx 0.02\eta_C$, which we attribute to the finite width of the passive level and to the fact that the competition of the two mechanisms unavoidably reduces the generated power, without necessarily reducing the transferred heat J_H .

The line cuts in Figs. 12(c)–12(f) show P and J_β , for different Γ_S . The same behavior that we observed for the current is shown here for the power: as we decrease the coupling to S, the quasiparticle contribution dominates and give $P > 0$ even close to the particle-hole symmetry point. The injected current from H is little affected. However, we observe that in the region with Cooper pair contributions (ε_p around the particle-hole symmetry point), J_H decreases with Γ_S , while it increases as quasiparticles take over (for larger $|\varepsilon_p|$), confirming the coherent nature of the reduction of J_H in the gap, in agreement with the pairing backaction effect identified in Sec. III. Note, however, that here we are in the regime $k_B T > \Gamma_S$.

Decreasing Γ_S suppresses the ER_N regions, as seen by comparing Figs. 12(c) and 12(e) for $\varepsilon_p \approx -0.4$ meV, as expected for a quasiparticle-only effect. For even more negative

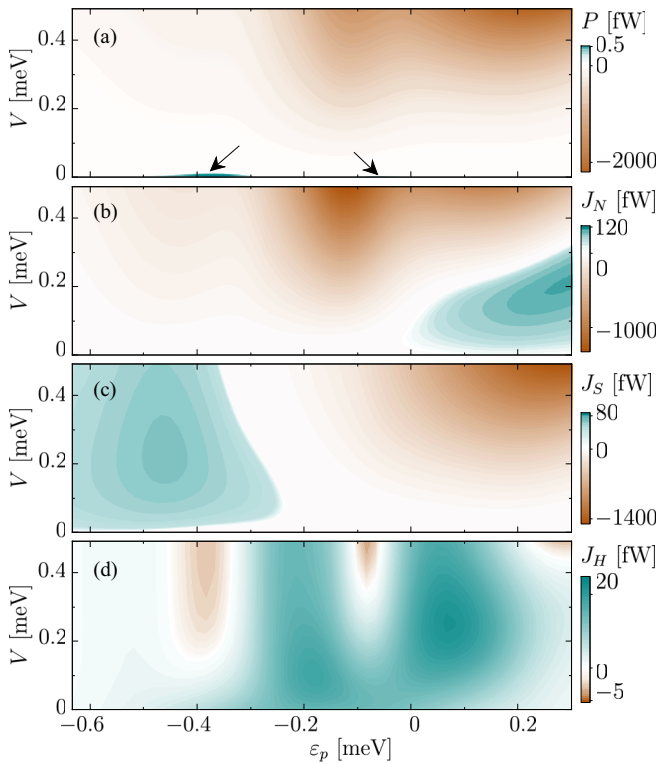


FIG. 13. Plots of (a) power, (b) J_N , (c) J_S and (d) J_H , as functions of the bias voltage V and the passive dot energy ε_p . Arrows in (a) indicate the regions where $P > 0$, shown in Fig. 12(a) for clarity. The same configuration as in Fig. 12 is considered, for a larger range of V . Note that the regions of $P > 0$ are almost invisible in (a) for being restricted to very low voltages.

ε_p , we find cooling of the superconductor induced by V , for small Γ_S , see Figs. 12(d) and 12(f). However, the operation ER_S is not found, which we attribute to the effect of the finite linewidth of the quantum dot states. We speculate that $P > 0$ and $J_S > 0$ may coexist for even smaller Γ_N and Γ_S . Unfortunately this will also considerably reduce the heat flows.

The currents in the presence of larger voltages are shown in Fig. 13. There, the charge current flowing in favor of the bias leads to power dissipation, $P < 0$. The arrows in Fig. 13(a) mark the regions where power is produced, as zoomed in in Fig. 12(a). Dissipation leads to heating terminal N, see Fig. 12(b), except for large and positive ε_p , where electrons tunnel from N into the passive dot over μ_N . Voltage also allows for the heat extracted from the superconductor to increase, see Fig. 13(c), again due to quasiparticles (we remind that Cooper pairs do not lead to heat flows, as discussed in Sec. III). Note the cooling power J_S is maximal for voltages of the order of the gap. This process is related to refrigerators based on normal-insulator-superconductor tunnel junctions [118], here mediated by the fluctuations in a quantum dot, see also Ref. [71]. Additionally, the dissipated Joule power reverts the heat flow at terminal H close to the gap borders, see Fig. 13(d) for $\varepsilon_p \approx -0.4$ meV and $\varepsilon_p \gtrsim 0.2$ meV, which makes the system work as a heat pump and recovers the $R_S P_H$ operation discussed in Sec. IV. Remarkably, for high enough V , we observe a subgap region (around $\varepsilon_p \approx -0.1$ meV)

where $J_H < 0$, i.e., induced by Andreev processes and their correlation with the charge fluctuations of the active dot.

VI. CONCLUSIONS

We have shown how a hybrid conductor composed by a quantum dot coupled to a normal and a superconductor contact can work as a quantum heat engine, when capacitively coupled to a second quantum dot in contact with a hot terminal. The injection of heat is mediated by the interaction of electrons in different dots, whose charge fluctuates. The asymmetry of the normal-superconductor contact induces a zero-bias current via two competing mechanisms: on one hand, the superconducting density of states acts as an efficient energy filter for quasiparticle tunneling. On the other hand, the hybridization of even parity states due to pairing depends on the occupation of the hot dot, hence changing the relative contribution of empty and doubly occupied states to the superposition and affecting the electron- or holelike character of the electrons tunneling from N. This way, the symmetry of a wave function is used as the piston of an autonomous quantum heat engine.

We have analyzed the limiting cases where these two contributions operate separately by using simple models described by quantum master equations. More realistic configurations where both effects coexist are treated numerically with NEGF techniques. The relative contribution of the two mechanisms can be controlled with gate voltages acting on the quantum dot levels. The contribution of Andreev processes dominates for states close to the chemical potential of the superconductor, while quasiparticle processes are enhanced for transitions via states aligned with the gap. The opposite contributions of the two mechanisms lead to changes of sign in the generated zero-bias current as the passive dot level is tuned which are not present in all-normal configurations [64,65]. The quantum coherent character of this mechanism manifests in an additional change of sign of the generated current as the active dot level is tuned. In this way, the coupled quantum dot acts not only as the heat source but also as an external knob of the response. We also identify a backaction of pairing on the active system in the form of a coherent pairing-Coulomb blockade of the injected heat current. The gap and the coherence peak in the superconducting DoS are beneficial for the conversion of heat into power, which reaches high efficiencies in the quasiparticle regime. Furthermore, it allows the system to work as a hybrid engine where several thermodynamic operations (power generation, cooling and/or heat pumping) coexist. Most of these features survive in the intermediate regime, where the finite linewidth of the quantum dot states introduces a limitation to the performance of the device. The robustness of the Andreev induced currents in this regime makes this system appealing for the experimental realization of quantum thermodynamic engines.

ACKNOWLEDGMENTS

We acknowledge P. Buset and G. Steffensen for useful comments. Work funded by Iran Science Elites Federation (ISEF) and by Spanish State Research Agency through Grants

No. PID2019-110125GB-I00, No. PID2020-117347GB-I00, No. PID2020-117671GB-I00, and No. RYC2016-20778 and through the Severo Ochoa and María de Maeztu Pro-

gram for Centers and Units of Excellence in R&D (No. MDM2017-0711 and No. CEX2018-000805-M) funded by MCIN/AEI/10.13039/501100011033.

- [1] G. Benenti, G. Casati, K. Saito, and R. S. Whitney, Fundamental aspects of steady-state conversion of heat to work at the nanoscale, *Phys. Rep.* **694**, 1 (2017).
- [2] F. Mazza, S. Valentini, R. Bosisio, G. Benenti, V. Giovannetti, R. Fazio, and F. Taddei, Separation of heat and charge currents for boosted thermoelectric conversion, *Phys. Rev. B* **91**, 245435 (2015).
- [3] V. L. Ginzburg, Thermoelectric effects in the superconducting state, *Sov. Phys. Usp.* **34**, 101 (1991).
- [4] G. Marchegiani, A. Braggio, and F. Giazotto, Nonlinear Thermoelectricity with Electron-Hole Symmetric Systems, *Phys. Rev. Lett.* **124**, 106801 (2020).
- [5] G. Marchegiani, A. Braggio, and F. Giazotto, Phase-tunable thermoelectricity in a Josephson junction, *Phys. Rev. Res.* **2**, 043091 (2020).
- [6] G. Germanese, F. Paolucci, G. Marchegiani, A. Braggio, and F. Giazotto, Bipolar thermoelectric Josephson engine, [arXiv:2202.02121](https://arxiv.org/abs/2202.02121).
- [7] D. Goury and R. Sánchez, Reversible thermal diode and energy harvester with a superconducting quantum interference single-electron transistor, *Appl. Phys. Lett.* **115**, 092601 (2019).
- [8] M. Kamp and B. Sothmann, Phase-dependent heat and charge transport through superconductor–quantum dot hybrids, *Phys. Rev. B* **99**, 045428 (2019).
- [9] A. G. Bauer and B. Sothmann, Phase-dependent transport in thermally driven superconducting single-electron transistors, *Phys. Rev. B* **104**, 195418 (2021).
- [10] Z. Cao, T.-F. Fang, L. Li, and H.-G. Luo, Thermoelectric-induced unitary Cooper pair splitting efficiency, *Appl. Phys. Lett.* **107**, 212601 (2015).
- [11] R. Sánchez, P. Buset, and A. L. Yeyati, Cooling by Cooper pair splitting, *Phys. Rev. B* **98**, 241414(R) (2018).
- [12] R. Hussein, M. Governale, S. Kohler, W. Belzig, F. Giazotto, and A. Braggio, Nonlocal thermoelectricity in a Cooper-pair splitter, *Phys. Rev. B* **99**, 075429 (2019).
- [13] N. S. Kirsanov, Z. B. Tan, D. S. Golubev, P. J. Hakonen, and G. B. Lesovik, Heat switch and thermoelectric effects based on Cooper-pair splitting and elastic cotunneling, *Phys. Rev. B* **99**, 115127 (2019).
- [14] Z. B. Tan, A. Laitinen, N. S. Kirsanov, A. Galda, V. M. Vinokur, M. Haque, A. Savin, D. S. Golubev, G. B. Lesovik, and P. J. Hakonen, Thermoelectric current in a graphene Cooper pair splitter, *Nat. Commun.* **12**, 138 (2021).
- [15] S. Verma and A. Singh, Non-equilibrium thermoelectric transport across normal metal–quantum dot–superconductor hybrid system within the Coulomb blockade regime, *J. Phys.: Condens. Matter* **34**, 155601 (2022).
- [16] P. Machon, M. Eschrig, and W. Belzig, Nonlocal Thermoelectric Effects and Nonlocal Onsager relations in a Three-Terminal Proximity-Coupled Superconductor-Ferromagnet Device, *Phys. Rev. Lett.* **110**, 047002 (2013).
- [17] F. Giazotto, J. W. A. Robinson, J. S. Moodera, and F. S. Bergeret, Proposal for a phase-coherent thermoelectric transistor, *Appl. Phys. Lett.* **105**, 062602 (2014).
- [18] A. Ozaeta, P. Virtanen, F. S. Bergeret, and T. T. Heikkilä, Predicted Very Large Thermoelectric Effect in Ferromagnet-Superconductor Junctions in the Presence of a Spin-Splitting Magnetic Field, *Phys. Rev. Lett.* **112**, 057001 (2014).
- [19] S.-Y. Hwang, R. López, and D. Sánchez, Large thermoelectric power and figure of merit in a ferromagnetic–quantum dot–superconducting device, *Phys. Rev. B* **94**, 054506 (2016).
- [20] S.-Y. Hwang, D. Sánchez, and R. López, A hybrid superconducting quantum dot acting as an efficient charge and spin Seebeck diode, *New J. Phys.* **18**, 093024 (2016).
- [21] S. Kolenda, M. J. Wolf, and D. Beckmann, Observation of Thermoelectric Currents in High-Field Superconductor-Ferromagnet Tunnel Junctions, *Phys. Rev. Lett.* **116**, 097001 (2016).
- [22] G. Marchegiani, P. Virtanen, F. Giazotto, and M. Campisi, Self-Oscillating Josephson Quantum Heat Engine, *Phys. Rev. Applied* **6**, 054014 (2016).
- [23] T. Savander, S. Tamura, C. Flindt, Y. Tanaka, and P. Buset, Thermoelectric detection of Andreev states in unconventional superconductors, *Phys. Rev. Res.* **2**, 043388 (2020).
- [24] F. Keidel, S.-Y. Hwang, B. Trauzettel, B. Sothmann, and P. Buset, On-demand thermoelectric generation of equal-spin Cooper pairs, *Phys. Rev. Res.* **2**, 022019(R) (2020).
- [25] G. Blasi, F. Taddei, L. Arrachea, M. Carrega, and A. Braggio, Nonlocal Thermoelectricity in a Superconductor–Topological-Insulator–Superconductor Junction in Contact with a Normal-Metal Probe: Evidence for Helical Edge States, *Phys. Rev. Lett.* **124**, 227701 (2020).
- [26] G. Blasi, F. Taddei, L. Arrachea, M. Carrega, and A. Braggio, Nonlocal thermoelectric engines in hybrid topological Josephson junctions, *Phys. Rev. B* **103**, 235434 (2021).
- [27] P. P. Hofer, J.-R. Souquet, and A. A. Clerk, Quantum heat engine based on photon-assisted Cooper pair tunneling, *Phys. Rev. B* **93**, 041418(R) (2016).
- [28] Ph. Jacquod and R. S. Whitney, Coherent thermoelectric effects in mesoscopic Andreev interferometers, *Europhys. Lett.* **91**, 67009 (2010).
- [29] M. S. Kalenkov and A. D. Zaikin, Large thermoelectric effect in ballistic Andreev interferometers, *Phys. Rev. B* **95**, 024518 (2017).
- [30] M. Nahum, T. M. Eiles, and J. M. Martinis, Electronic microrefrigerator based on a normal-insulator-superconductor tunnel junction, *Appl. Phys. Lett.* **65**, 3123 (1994).
- [31] M. M. Leivo, J. P. Pekola, and D. V. Averin, Efficient Peltier refrigeration by a pair of normal metal/insulator/superconductor junctions, *Appl. Phys. Lett.* **68**, 1996 (1996).
- [32] M. Marín-Suárez, J. T. Peltonen, D. S. Golubev, and J. P. Pekola, An electron turnstile for frequency-to-power conversion, *Nat. Nanotechnol.* **17**, 239 (2022).

- [33] J. P. Pekola, M. Marín-Suárez, T. Pyhäranta, and B. Karimi, Ultimate Accuracy of Frequency to Power Conversion by Single-Electron Injection, *Phys. Rev. Lett.* **129**, 037702 (2022).
- [34] R. Sánchez and M. Büttiker, Optimal energy quanta to current conversion, *Phys. Rev. B* **83**, 085428 (2011).
- [35] B. Sothmann, R. Sánchez, A. N. Jordan, and M. Büttiker, Rectification of thermal fluctuations in a chaotic cavity heat engine, *Phys. Rev. B* **85**, 205301 (2012).
- [36] H. Thierschmann, R. Sánchez, B. Sothmann, F. Arnold, C. Heyn, W. Hansen, H. Buhmann, and L. W. Molenkamp, Three-terminal energy harvester with coupled quantum dots, *Nat. Nanotechnol.* **10**, 854 (2015).
- [37] F. Hartmann, P. Pfeffer, S. Höfling, M. Kamp, and L. Worschech, Voltage Fluctuation to Current Converter with Coulomb-Coupled Quantum Dots, *Phys. Rev. Lett.* **114**, 146805 (2015).
- [38] B. Roche, P. Roulleau, T. Jullien, Y. Jompol, I. Farrer, D. A. Ritchie, and D. C. Glatli, Harvesting dissipated energy with a mesoscopic ratchet, *Nat. Commun.* **6**, 6738 (2015).
- [39] H. Thierschmann, F. Arnold, M. Mittermüller, L. Maier, C. Heyn, W. Hansen, H. Buhmann, and L. W. Molenkamp, Thermal gating of charge currents with Coulomb coupled quantum dots, *New J. Phys.* **17**, 113003 (2015).
- [40] B. Rutten, M. Esposito, and B. Cleuren, Reaching optimal efficiencies using nanosized photoelectric devices, *Phys. Rev. B* **80**, 235122 (2009).
- [41] O. Entin-Wohlman, Y. Imry, and A. Aharony, Three-terminal thermoelectric transport through a molecular junction, *Phys. Rev. B* **82**, 115314 (2010).
- [42] T. Krause, G. Schaller, and T. Brandes, Incomplete current fluctuation theorems for a four-terminal model, *Phys. Rev. B* **84**, 195113 (2011).
- [43] B. Sothmann and M. Büttiker, Magnon-driven quantum-dot heat engine, *Europhys. Lett.* **99**, 27001 (2012).
- [44] T. Ruokola and T. Ojanen, Theory of single-electron heat engines coupled to electromagnetic environments, *Phys. Rev. B* **86**, 035454 (2012).
- [45] J.-H. Jiang, O. Entin-Wohlman, and Y. Imry, Thermoelectric three-terminal hopping transport through one-dimensional nanosystems, *Phys. Rev. B* **85**, 075412 (2012).
- [46] C. Bergenfeldt, P. Samuelsson, B. Sothmann, C. Flindt, and M. Büttiker, Hybrid Microwave-Cavity Heat Engine, *Phys. Rev. Lett.* **112**, 076803 (2014).
- [47] L. Arrachea, N. Bode, and F. von Oppen, Vibrational cooling and thermoelectric response of nanoelectromechanical systems, *Phys. Rev. B* **90**, 125450 (2014).
- [48] R. Bosisio, G. Fleury, J.-L. Pichard, and C. Gorini, Nanowire-based thermoelectric ratchet in the hopping regime, *Phys. Rev. B* **93**, 165404 (2016).
- [49] K. Yamamoto, O. Entin-Wohlman, A. Aharony, and N. Hatano, Efficiency bounds on thermoelectric transport in magnetic fields: The role of inelastic processes, *Phys. Rev. B* **94**, 121402(R) (2016).
- [50] J.-H. Jiang and Y. Imry, Enhancing Thermoelectric Performance Using Nonlinear Transport Effects, *Phys. Rev. Applied* **7**, 064001 (2017).
- [51] S. Dorsch, A. Svilans, M. Josefsson, B. Goldozián, M. Kumar, C. Thelander, A. Wacker, and A. Burke, Heat Driven Transport in Serial Double Quantum Dot Devices, *Nano Lett.* **21**, 988 (2021).
- [52] S. Dorsch, S. Fahlvik, and A. Burke, Characterization of electrostatically defined bottom-heated InAs nanowire quantum dot systems, *New J. Phys.* **23**, 125007 (2021).
- [53] A. N. Jordan, B. Sothmann, R. Sánchez, and M. Büttiker, Powerful and efficient energy harvester with resonant-tunneling quantum dots, *Phys. Rev. B* **87**, 075312 (2013).
- [54] F. Mazza, R. Bosisio, G. Benenti, V. Giovannetti, R. Fazio, and F. Taddei, Thermoelectric efficiency of three-terminal quantum thermal machines, *New J. Phys.* **16**, 085001 (2014).
- [55] S. Donsa, S. Andergassen, and K. Held, Double quantum dot as a minimal thermoelectric generator, *Phys. Rev. B* **89**, 125103 (2014).
- [56] J.-H. Jiang, Enhancing efficiency and power of quantum-dots resonant tunneling thermoelectrics in three-terminal geometry by cooperative effects, *J. Appl. Phys.* **116**, 194303 (2014).
- [57] G. Jaliel, R. K. Puddy, R. Sánchez, A. N. Jordan, B. Sothmann, I. Farrer, J. P. Griffiths, D. A. Ritchie, and C. G. Smith, Experimental Realization of a Quantum Dot Energy Harvester, *Phys. Rev. Lett.* **123**, 117701 (2019).
- [58] L. W. Molenkamp, K. Flensberg, and M. Kemerink, Scaling of the Coulomb Energy Due to Quantum Fluctuations in the Charge on a Quantum Dot, *Phys. Rev. Lett.* **75**, 4282 (1995).
- [59] I. H. Chan, R. M. Westervelt, K. D. Maranowski, and A. C. Gossard, Strongly capacitively coupled quantum dots, *Appl. Phys. Lett.* **80**, 1818 (2002).
- [60] A. Hübel, J. Weis, W. Dietsche, and K. v. Klitzing, Two laterally arranged quantum dot systems with strong capacitive interdot coupling, *Appl. Phys. Lett.* **91**, 102101 (2007).
- [61] D. T. McClure, L. DiCarlo, Y. Zhang, H.-A. Engel, C. M. Marcus, M. P. Hanson, and A. C. Gossard, Tunable Noise Cross Correlations in a Double Quantum Dot, *Phys. Rev. Lett.* **98**, 056801 (2007).
- [62] P. Strasberg, G. Schaller, T. Brandes, and M. Esposito, Thermodynamics of a Physical Model Implementing a Maxwell Demon, *Phys. Rev. Lett.* **110**, 040601 (2013).
- [63] Y. Zhang, Y. Wang, C. Huang, G. Lin, and J. Chen, Thermoelectric performance and optimization of three-terminal quantum dot nano-devices, *Energy* **95**, 593 (2016).
- [64] A.-M. Daré and P. Lombardo, Powerful Coulomb-drag thermoelectric engine, *Phys. Rev. B* **96**, 115414 (2017).
- [65] N. Walldorf, A.-P. Jauho, and K. Kaasbjerg, Thermoelectrics in Coulomb-coupled quantum dots: Cotunneling and energy-dependent lead couplings, *Phys. Rev. B* **96**, 115415 (2017).
- [66] P. Strasberg, G. Schaller, T. L. Schmidt, and M. Esposito, Fermionic reaction coordinates and their application to an autonomous Maxwell demon in the strong-coupling regime, *Phys. Rev. B* **97**, 205405 (2018).
- [67] R. D. Mayrhofer, C. Elouard, J. Splettstoesser, and A. N. Jordan, Stochastic thermodynamic cycles of a mesoscopic thermoelectric engine, *Phys. Rev. B* **103**, 075404 (2021).
- [68] R. Sánchez, B. Sothmann, A. N. Jordan, and M. Büttiker, Correlations of heat and charge currents in quantum-dot thermoelectric engines, *New J. Phys.* **15**, 125001 (2013).
- [69] Y. Zhang, G. Lin, and J. Chen, Three-terminal quantum-dot refrigerators, *Phys. Rev. E* **91**, 052118 (2015).
- [70] J. V. Koski, A. Kutvonen, I. M. Khaymovich, T. AlaNissila, and J. P. Pekola, On-Chip Maxwell's Demon as

- an Information-Powered Refrigerator, *Phys. Rev. Lett.* **115**, 260602 (2015).
- [71] R. Sánchez, Correlation-induced refrigeration with superconducting single-electron transistors, *Appl. Phys. Lett.* **111**, 223103 (2017).
- [72] P. A. Erdman, B. Bhandari, R. Fazio, J. P. Pekola, and F. Taddei, Absorption refrigerators based on Coulomb-coupled single-electron systems, *Phys. Rev. B* **98**, 045433 (2018).
- [73] A.-M. Daré, Comparative study of heat-driven and power-driven refrigerators with Coulomb-coupled quantum dots, *Phys. Rev. B* **100**, 195427 (2019).
- [74] N. A. Mortensen, K. Flensberg, and A.-P. Jauho, Coulomb Drag in Coherent Mesoscopic Systems, *Phys. Rev. Lett.* **86**, 1841 (2001).
- [75] V. S. Khrapai, S. Ludwig, J. P. Kotthaus, H. P. Tranitz, and W. Wegscheider, Double-Dot Quantum Ratchet Driven by an Independently Biased Quantum Point Contact, *Phys. Rev. Lett.* **97**, 176803 (2006).
- [76] U. Gasser, S. Gustavsson, B. Küng, K. Ensslin, T. Ihn, D. C. Driscoll, and A. C. Gossard, Statistical electron excitation in a double quantum dot induced by two independent quantum point contacts, *Phys. Rev. B* **79**, 035303 (2009).
- [77] G. Shinkai, T. Hayashi, T. Ota, K. Muraki, and T. Fujisawa, Bidirectional current drag induced by two-electron cotunneling in coupled double quantum dots, *Appl. Phys. Express* **2**, 081101 (2009).
- [78] V. Moldoveanu and B. Tanatar, Coulomb drag in parallel quantum dots, *Europhys. Lett.* **86**, 67004 (2009).
- [79] R. Sánchez, R. López, D. Sánchez, and M. Büttiker, Mesoscopic Coulomb Drag, Broken Detailed Balance, and Fluctuation Relations, *Phys. Rev. Lett.* **104**, 076801 (2010).
- [80] R. Hussein and S. Kohler, Coherent quantum ratchets driven by tunnel oscillations: Fluctuations and correlations, *Phys. Rev. B* **86**, 115452 (2012).
- [81] R. Hussein and S. Kohler, Capacitively coupled nano conductors, *Ann. Phys.* **527**, 610 (2015).
- [82] D. Bischoff, M. Eich, O. Zilberberg, C. Rössler, T. Ihn, and K. Ensslin, Measurement back-action in stacked graphene quantum dots, *Nano Lett.* **15**, 6003 (2015).
- [83] K. Kaasbjerg and A.-P. Jauho, Correlated Coulomb Drag in Capacitively Coupled Quantum-Dot Structures, *Phys. Rev. Lett.* **116**, 196801 (2016).
- [84] A. J. Keller, J. S. Lim, D. Sánchez, R. López, S. Amasha, J. A. Katine, H. Shtrikman, and D. Goldhaber-Gordon, Cotunneling Drag Effect in Coulomb-Coupled Quantum Dots, *Phys. Rev. Lett.* **117**, 066602 (2016).
- [85] J. S. Lim, D. Sánchez, and R. López, Engineering drag currents in Coulomb coupled quantum dots, *New J. Phys.* **20**, 023038 (2018).
- [86] M. A. Sierra, D. Sánchez, A.-P. Jauho, and K. Kaasbjerg, Fluctuation-driven Coulomb drag in interacting quantum dot systems, *Phys. Rev. B* **100**, 081404(R) (2019).
- [87] S. Takada, G. Georgiou, E. Arrighi, H. Edlbauer, Y. Okazaki, S. Nakamura, A. Ludwig, A. D. Wieck, M. Yamamoto, C. Bäuerle, and N.-H. Kaneko, Heat-driven electron-motion in a nanoscale electronic circuit, *J. Phys. Soc. Jpn.* **90**, 113707 (2021).
- [88] B. N. Narozhny and A. Levchenko, Coulomb drag, *Rev. Mod. Phys.* **88**, 025003 (2016).
- [89] R. S. Whitney, R. Sánchez, F. Haupt, and J. Splettstoesser, Thermoelectricity without absorbing energy from the heat sources, *Phys. E* **75**, 257 (2016).
- [90] J.-T. Lü, J.-S. Wang, P. Hedegård, and M. Brandbyge, Electron and phonon drag in thermoelectric transport through coherent molecular conductors, *Phys. Rev. B* **93**, 205404 (2016).
- [91] B. Bhandari, G. Chiriacò, P. A. Erdman, R. Fazio, and F. Taddei, Thermal drag in electronic conductors, *Phys. Rev. B* **98**, 035415 (2018).
- [92] P. Ben-Abdallah, Thermal photon drag in many-body systems, *Phys. Rev. B* **99**, 201406(R) (2019).
- [93] R. Sánchez, P. Samuelsson, and P. P. Potts, Autonomous conversion of information to work in quantum dots, *Phys. Rev. Res.* **1**, 033066 (2019).
- [94] W. Berdanier, T. Scaffidi, and J. E. Moore, Energy Drag in Particle-Hole Symmetric Systems as a Quantum Quench, *Phys. Rev. Lett.* **123**, 246603 (2019).
- [95] J. Lu, J.-H. Jiang, and Y. Imry, Unconventional four-terminal thermoelectric transport due to inelastic transport: Cooling by transverse heat current, transverse thermoelectric effect, and Maxwell demon, *Phys. Rev. B* **103**, 085429 (2021).
- [96] M. Xi, R. Wang, J. Lu, and J.-H. Jiang, Coulomb thermoelectric drag in four-terminal mesoscopic quantum transport, *Chin. Phys. Lett.* **38**, 088801 (2021).
- [97] L. Wang, Z. Wang, C. Wang, and J. Ren, Cycle Flux Ranking of Network Analysis in Quantum Thermal Devices, *Phys. Rev. Lett.* **128**, 067701 (2022).
- [98] E. G. Idrisov, I. P. Levkivskiy, and E. V. Sukhorukov, Thermal drag effect in quantum Hall circuits, [arXiv:2203.02558](https://arxiv.org/abs/2203.02558).
- [99] D. Venturelli, R. Fazio, and V. Giovannetti, Minimal Self-Contained Quantum Refrigeration Machine Based on Four Quantum Dots, *Phys. Rev. Lett.* **110**, 256801 (2013).
- [100] S. M. Tabatabaei, D. Sánchez, A. L. Yeyati, and R. Sánchez, Andreev-Coulomb Drag in Coupled Quantum Dots, *Phys. Rev. Lett.* **125**, 247701 (2020).
- [101] M. R. Gräber, T. Nussbaumer, W. Belzig, and C. Schönberger, Quantum dot coupled to a normal and a superconducting lead, *Nanotechnology* **15**, S479 (2004).
- [102] R. S. Deacon, Y. Tanaka, A. Oiwa, R. Sakano, K. Yoshida, K. Shibata, K. Hirakawa, and S. Tarucha, Tunneling Spectroscopy of Andreev Energy Levels in a Quantum Dot Coupled to a Superconductor, *Phys. Rev. Lett.* **104**, 076805 (2010).
- [103] S. De Franceschi, L. Kouwenhoven, C. Schönberger, and W. Wernsdorfer, Hybrid superconductor-quantum dot devices, *Nat. Nanotechnol.* **5**, 703 (2010).
- [104] G. Manzano, R. Sánchez, R. Silva, G. Haack, J. B. Brask, N. Brunner, and P. P. Potts, Hybrid thermal machines: Generalized thermodynamic resources for multitasking, *Phys. Rev. Res.* **2**, 043302 (2020).
- [105] O. Entin-Wohlman, Y. Imry, and A. Aharony, Enhanced performance of joint cooling and energy production, *Phys. Rev. B* **91**, 054302 (2015).
- [106] K. Hammam, H. Leitch, Y. Hassouni, and G. De Chiara, Exploiting coherence for quantum thermodynamic advantage, [arXiv:2202.07515](https://arxiv.org/abs/2202.07515).
- [107] G. Schaller, *Open Quantum Systems Far from Equilibrium* (Springer, Cham, Switzerland, 2014).
- [108] P. Strasberg, *Quantum Stochastic Thermodynamics* (Oxford University Press, Oxford, 2022).

- [109] H. Haug and A.-P. Jauho, *Quantum Kinetics in Transport and Optics of Semiconductors* (Springer, Berlin, 2008).
- [110] A. V. Rozhkov and D. P. Arovas, Interacting-impurity Josephson junction: Variational wave functions and slave-boson mean-field theory, *Phys. Rev. B* **62**, 6687 (2000).
- [111] P. Trocha and J. Barnaś, Spin-polarized Andreev transport influenced by Coulomb repulsion through a two-quantum-dot system, *Phys. Rev. B* **89**, 245418 (2014).
- [112] S. E. Nigg, R. P. Tiwari, S. Walter, and T. L. Schmidt, Detecting nonlocal Cooper pair entanglement by optical Bell inequality violation, *Phys. Rev. B* **91**, 094516 (2015).
- [113] W. G. van der Wiel, S. De Franceschi, J. M. Elzerman, T. Fujisawa, S. Tarucha, and L. P. Kouwenhoven, Electron transport through double quantum dots, *Rev. Mod. Phys.* **75**, 1 (2002).
- [114] L. P. Kouwenhoven, C. M. Marcus, P. L. McEuen, S. Tarucha, R. M. Westervelt, and N. S. Wingreen, Electron transport in quantum dots, in *Mesoscopic Electron Transport*, edited by L. L. Sohn, L. P. Kouwenhoven, and G. Schön (Springer Netherlands, Dordrecht, 1997), pp. 105–214.
- [115] R. C. Dynes, V. Narayanamurti, and J. P. Garno, Direct Measurement of Quasiparticle-Lifetime Broadening in a Strong-Coupled Superconductor, *Phys. Rev. Lett.* **41**, 1509 (1978).
- [116] H. L. Edwards, Q. Niu, and A. L. de Lozanne, A quantum-dot refrigerator, *Appl. Phys. Lett.* **63**, 1815 (1993).
- [117] J. R. Prance, C. G. Smith, J. P. Griffiths, S. J. Chorley, D. Anderson, G. A. C. Jones, I. Farrer, and D. A. Ritchie, Electronic Refrigeration of a Two-Dimensional Electron Gas, *Phys. Rev. Lett.* **102**, 146602 (2009).
- [118] F. Giazotto, T. T. Heikkilä, A. Luukanen, A. M. Savin, and J. P. Pekola, Opportunities for mesoscopics in thermometry and refrigeration: Physics and applications, *Rev. Mod. Phys.* **78**, 217 (2006).